

Accepted Manuscript

Title: Preparation and Reactivity of UV Light-Reduced Pd/ α -Fe₂O₃ Catalyst Towards the Hydrogenation of o-Chloronitrobenzene

Author: Weidong Jiang Bin Xu Zhen Xiang Xiaoqiang Liu Fuan Liu



PII: S0926-860X(16)30177-6
DOI: <http://dx.doi.org/doi:10.1016/j.apcata.2016.04.007>
Reference: APCATA 15835

To appear in: *Applied Catalysis A: General*

Received date: 5-2-2016
Revised date: 9-4-2016
Accepted date: 11-4-2016

Please cite this article as: Weidong Jiang, Bin Xu, Zhen Xiang, Xiaoqiang Liu, Fuan Liu, Preparation and Reactivity of UV Light-Reduced Pd/ α -Fe₂O₃ Catalyst Towards the Hydrogenation of o-Chloronitrobenzene, *Applied Catalysis A, General* <http://dx.doi.org/10.1016/j.apcata.2016.04.007>

This is a PDF file of an unedited manuscript that has been accepted for publication. As a service to our customers we are providing this early version of the manuscript. The manuscript will undergo copyediting, typesetting, and review of the resulting proof before it is published in its final form. Please note that during the production process errors may be discovered which could affect the content, and all legal disclaimers that apply to the journal pertain.

Preparation and Reactivity of UV Light-Reduced Pd/ α -Fe₂O₃ Catalyst Towards the Hydrogenation of *o*-Chloronitrobenzene

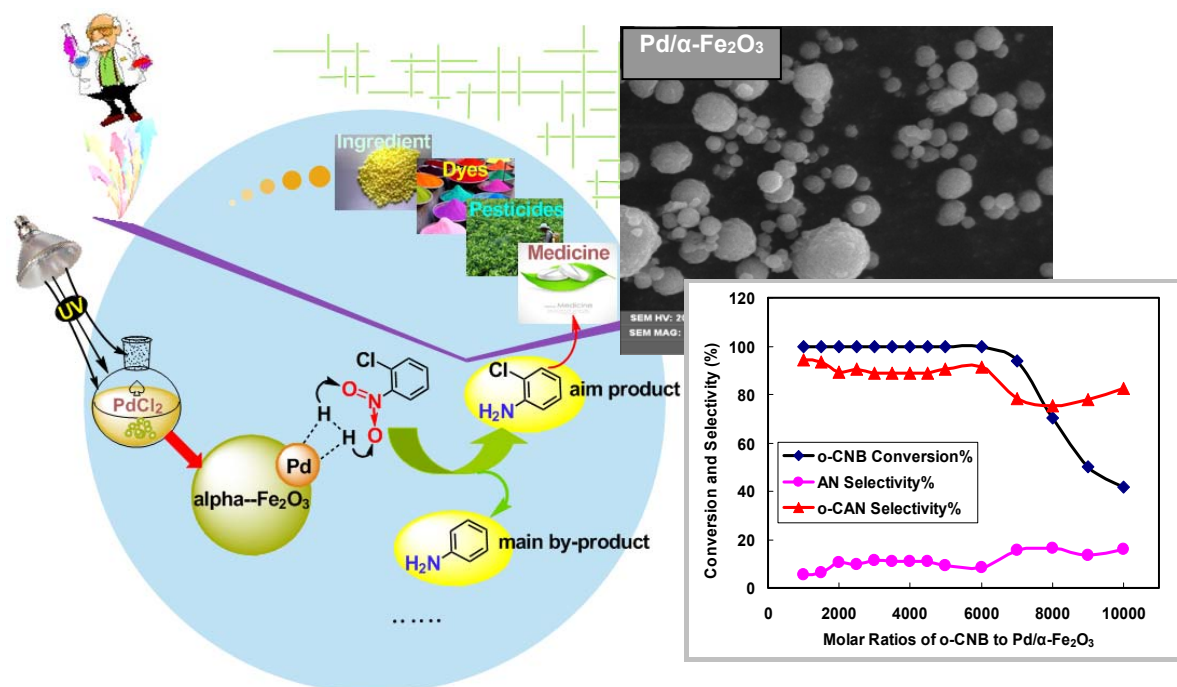
Weidong Jiang^{a, b*}, Bin Xu^{a, b}, Zhen Xiang^{a, b}, Xiaoqiang Liu^{a, b}, Fuan Liu^b

(¹ School of Chemical and Pharmaceutical Engineering, Sichuan University of Science & Engineering, Zigong 643000, China;

² Key Laboratory of Green Catalysis of Sichuan Institute of High Education, Zigong 643000, China)

Graphical abstract

The present work reported the convenient preparation of Pd-based catalyst over α -Fe₂O₃ as support via a UV light-induced reduction process. The resulting Pd/ α -Fe₂O₃ catalyst exhibited good performance for the hydrogenation reduction of o-chloronitrobenzene (o-CNB), yielding completely o-CNB conversion and 91.4% selectivity of o-CAN at high substrate/catalyst ratio (6000:1) under mild conditions.



HIGHLIGHTS

- Pd/ α -Fe₂O₃ catalyst was prepared by a convenient UV light-induced reduction.
- Pd/ α -Fe₂O₃ maintained good reactivity towards o-CNB hydrogenation at high o-CNB/Pd ratios up to 7000.
- Pd/ α -Fe₂O₃-promoted o-CNB hydrogenation gave 100% o-CNB conversion and 91.4% o-CAN selectivity under mild conditions.

Abstract: A type of Pd/ α -Fe₂O₃ catalyst was synthesized by a convenient UV light-induced reduction in the presence of Fe³⁺ ions. The synthesized Pd/ α -Fe₂O₃ particles were characterized by X-ray diffraction (XRD), low-resolution transmission electron microscopy (TEM), high-resolution transmission electron microscopy (HR-TEM), X-ray photoelectron spectrum (XPS), atomic force microscope (AFM), scan electron microscopy with energy dispersion spectra (SEM-EDS), FT-IR and BET. Related characterizations confirm that UV light-induced reduction is a feasible, simply and environment-friendly method for the preparation of supported catalysts containing active metal. Furthermore, hydrogenation of o-chloronitrobenzene (o-CNB) to o-chloroaniline (o-CAN) by the selected Pd(0.5%)/ α -Fe₂O₃ was investigated systematically. The α -Fe₂O₃-supported Pd catalyst was found to exhibit good catalytic activity and selectivity for the o-CNB reduction under mild conditions. The hydrogenation of o-CNB over the resulting Pd-based catalyst gave a 100% o-CNB conversion and 91.4% selectivity of o-CAN under the reaction conditions of 50 °C, 2 hrs, 1MPa hydrogen pressure, n_{o-CNB}/n_{Pd}=6000:1. Moreover, the resulting Pd-based catalyst remained higher hydrogenation reactivity after three runs even if a sharply decrease in activity was observed at the fourth run. The obtained results reveal the as-prepared Pd/ α -Fe₂O₃ is an efficient catalyst for the hydrogenation of o-CNB even at a high level of substrate concentration.

Keywords: catalytic hydrogenation, o-chloronitrobenzene, UV light-induced reduction, Pd/ α -Fe₂O₃ catalyst

1. Introduction

The hydrogenation of nitro compounds is commonly conducted to prepare aromatic amines that are important intermediates for dyes, drugs, and agrochemicals [1, 2]. Thereupon, many research groups have engaged in the synthetic methods and process of aromatic amines [3]. Especially, the hydrogenation of corresponding nitroaromatics proved to be an easier and convenient route for the production of aromatic amines [4-13]. Hence, many chemists and researchers devoted to the development and improvement of this technology.

For one catalytic reaction two main aspects, including developing efficient catalysts and optimizing reaction conditions, are highly attracted scientist's attention. Noble metal catalysts are well known for their high catalytic activities in hydrogenation reactions [5, 7, 14-19]. Among these catalysts, palladium-based catalysts were widely used in the reduction of various compounds due to its high activity and selectivity [20-26]. To improve the stability and recyclability of metal catalysts, moreover, almost all active metal components applied in previous works were loaded on the varied supports, such as activated carbon [27], metallic or non-metallic oxidates [15, 28-30], polymer [31, 32], grapheme [33], etc. At present, chemists focused on the design and preparation of different supports with dazzling morphologies.

In the catalytic hydrogenation reactions, it was widely accepted that zero-valent metal atoms on the carriers are the real catalysts. This is the reason for a reduction process of cationic metals in the preparation of immobilized metal catalysts. Nowadays, chemical reductants [34, 35] were applied in the reduction of metal cations to zero-valent ones. Compressed hydrogen as classic reducing agent is used to reduce metal ions loaded on supports [36], and whereas it is potential flammable and explosive owing to its intrinsic characters. Meanwhile, in the general preparation of supported metal catalysts, chemical reductants are widely applied in the reduction of metal ions. Howbeit, these reductants have their limitations concerning expensive price, environmental hazard and operated dangerous.

Interestingly, Enrico Borgarello *et. al* reported a facile UV light-induced reduction method [37] for the reduction of metal ions. Nevertheless, this strategy was seldom used in the preparation of various supported catalysts for the hydrogenation reaction so far. In the present study, we prepared a kind of immobilized Pd catalyst over stable α -Fe₂O₃ using UV light-induced reduction method as a facile and environment-friendly one in comparison with chemical reduction. Furthermore, we evaluated the hydrogenation reactivity of the resulting Pd-base catalyst, systematically. Impact of varied reaction conditions on the hydrogenation was screened for the aim of achieving much

higher o-CAN yield.

2. Experimental

2.1 Material and Methods

All reagents were of analytical grade and used as received. $\text{PdCl}_2 \cdot 2\text{H}_2\text{O}$ was a product of Kunming Institute of Precious Metals (China). $\text{Fe}(\text{NO}_3)_3 \cdot 9\text{H}_2\text{O}$ was purchased from Tianjin Fuchen Chemical Reagents Factory (China). Standard samples of o-CNB, o-CAN and aniline were purchased from Sigma-Aldrich Co.

Preparation of $\alpha\text{-Fe}_2\text{O}_3$. The $\alpha\text{-Fe}_2\text{O}_3$ carriers were obtained according to following process. $\text{Fe}(\text{NO}_3)_3 \cdot 9\text{H}_2\text{O}$ solution (0.1mol/L) was prepared in deionized water. Ammonia solution was slowly dropped into the $\text{Fe}(\text{NO}_3)_3 \cdot 9\text{H}_2\text{O}$ solution using constant-flow pump with stirring, during which the pH value of the mixture was adjusted to 8 ~9. Afterwards, the mixed solution was heated to remove the residual ammonia. The mixture was cooled down to room temperature, and filtrated under vacuum along with a washing process with anhydrous ethanol. The yielded solid was dried under vacuum at 80^oC for 4 hrs. Furthermore, the dried solid was calcinated in a muffle furnace at 250^oC for 2 hrs. Ultimately, the desired brown $\alpha\text{-Fe}_2\text{O}_3$ powder sample was obtained via grinding operation.

Preparation of Pd/ $\alpha\text{-Fe}_2\text{O}_3$ using facial UV-light reduction route. $\alpha\text{-Fe}_2\text{O}_3$ powder was added to the prepared solution of $\text{PdCl}_2 \cdot 2\text{H}_2\text{O}$ (theroretic Pd loading content 0.5%). The mixture was stirred thoroughly under ultraviolet radiation ^[37] (30W) with a constant wavelength of 365nm for 24 hrs. The mixture was filtered and washed with deionized water. The solids obtained were dried in vaccum at 80^oC for 4 hrs. And then, grinding the dried solids produced the desired $\alpha\text{-Fe}_2\text{O}_3$ -supported Pd catalyst.

2.2 Structural and Morphologic Characterizations

Low resolution TEM (JEOL JEM 1200EX working at 100 kV) and high-resolution TEM (FEI Tecnai G2 F20 S-Twin working at 200 kV) were utilized to characterize the morphology of the Pd/ $\alpha\text{-Fe}_2\text{O}_3$ catalyst. BET areas were recorded on a SSA-4200 Specific Surface Area and Porosity Analyzer (Beijing Builder Electronic Technology Co., Ltd.) with a 30% v/v N_2/H_2 flow using pure N_2 (99.9%) as an internal standard. The crystalline phase of the as-prepared Pd catalyst was recorded on a Bruker D2-PHASER X-ray diffractometer (Germany Bruker AXE) with nickel-filtered Cu K α radiation ($\lambda = 1.5417 \text{ \AA}$, 40kV, 25mA) in the 2 θ zone of 10-90^o, and with a scan speed of 0.06^o/sec. Atom Force Microscope (AFM) images were obtained on an E-SWEEP

AFM (Hitachi High-Technologies Co., Japan). Scanning Electron Microscope with an EDS detector (Germany Bruker AXE) was measured on a VEGA 3SBU instrument from Tescan Co., Czech Republic. The loading content of Pd metal on the resulting Pd-base catalyst was determined on Spectro Arcos ICP-OES (Germany Spectro Analysis Co., Ltd).

2.3 Catalytic Tests

The catalytic hydrogenation of o-CNB was preformed in a 100ml GYF-60-2 stainless-steel autoclave (China Weihai Autocontrolled Autoclave Ltd.) with a thermocouple and a mechanical stirrer. Reaction reagents and catalyst were added into the stainless-steel reactor before each run. The hydrogenation reaction of o-CNB started after the reaction system was heated to the desired temperature.

2.4 Analytical Methods for the Products

The reaction mixtures were filtrated before the product analysis. The analysis of the obtained organic phase was performed using a SC-3000B-204 gas chromatography (Chongqing Chuanyi Analyzer Co., LTD, China) equipped with a flame ionization detector (FID) and an SE-54 capillary column (30m×Φ0.53mm). The oven temperature was tuned to 150 °C, while injector temperature and detector temperature were respectively 260°C and 220°C. The column temperature was progressively increased from 100°C (3min) to 220°C (6min) with a heating rate of 35°C/min. Data processing was performed with an HW-2000 chromatography workstation (Nanjing Qianpu Software, China). The major reactant and products were identified by comparison with corresponding authentic samples.

3 Results and Discussions

3.1 Varied Characterizations of the As-prepared Pd/ α -Fe₂O₃ Catalyst

To elucidate the structure-activity relation of the synthesized Pd catalyst, it is highly important that the structure characterizations by some classic physical methods, such as XRD, SEM, element mapping, TEM, XPS, AFM, etc. As shown in Fig. 1, it was found that the crystalline phase of Pd/ α -Fe₂O₃ catalyst is almost the same as that of the used support, α -Fe₂O₃. The X-ray diffraction peak of nano α -Fe₂O₃ at $2\theta=24.16^\circ$, 33.11° , 35.62° , 40.86° , 49.46° , 54.11° , 57.60° , 62.34° , 64.02° , 71.89° , and 75.34° are assigned to the scattering from (012), (104), (110), (113), (024), (116), (018), (214), (300), (101), and (220) planes and well match with the JCPDS card no.89-596. No

crystal phase of Pd was detected by XRD analysis, which is mainly due to two reasons. The one is that the particle size of the Pd(0) species were too small to be detected as well the metallic Pd(0) exhibited amorphous-like or less ordered structural features. Another one is that high dispersion of metallic Pd (0) on the surface of supports leads to no characteristic peaks of metal species that can be used for the observation in the XRD spectra. Therefore, average crystallite sizes of metallic Pd species cannot be estimated on the basis of the XRD patterns using the Scherrer equation.

The SEM images of α -Fe₂O₃ powder and Pd/ α -Fe₂O₃ catalyst were shown in Fig. 2. The Pd/ α -Fe₂O₃ powders display spherical morphography (Fig. 2B) which is highly accordance with those of α -Fe₂O₃ powders (Fig. 2A). From the SEM images, the powder sizes distribute in a range of 0.5 to 5.0 μ m. And, the size distribution of most of Pd/ α -Fe₂O₃ powders are in the range from 1.0 to 1.5 μ m. Moreover, TEM images (Figs. 2C and 2D) denote that those Pd/ α -Fe₂O₃ powders are aggregates of nano α -Fe₂O₃ crystallites on which catalytic Pd particles are loaded. One can observe that each one α -Fe₂O₃ crystal particle possesses rice-like morphography with almost uniform size of 10nm \times 8nm \times 8nm. Fig. 2D also shows the Pd particals were successfully loaded on the surface of α -Fe₂O₃. The crystallite size of Pd partical is found to be about 6nm \times 4nm \times 4nm, which can be also confirmed by the high-resolution TEM (Fig. 2E) of Pd catalyst over α -Fe₂O₃. The interplanar spacing of the {200} plane of metallic Pd(0) shown in Fig. 2E is determined as aproximate 0.19 nm, which is consistent with the reported figure [38]. Furthermore, the selected area electron diffraction pattern (SAED) (Fig. 2F) of Pd/ α -Fe₂O₃ catalyst displays a concentric circling diffraction character, indicating the polycrystalline microstructure of the resulting supported Pd catalyst. This fact is highly in agreement with the results of HR-TEM shown in Figs. 2C and 2D.

The X-ray photoelectron spectrum (XPS) was obtained to analyze the valence state of metal element and the surface chemical composition of the Pd/ α -Fe₂O₃ catalyst. Fig. 3A displays the total XPS spectra of Pd3d, Fe2p, O1s and C1s, respectively. The spectrum of C1s can be neglected because of the adsorbed carbon dioxide in air. The XPS binding energies (BE) for Pd (0) 3d are at 335.0 eV (3d_{5/2}) and 340.0 eV (3d_{3/2}) as reported in literature [39, 40]. As shown in Fig. 2B, the BE of Pd3d_{5/2} level in Pd/ α -Fe₂O₃ is about 337.0 eV, which is 2.0 eV higher than that (= 335.0 eV) of the standard zero-valent state of Pd. The peak at 342 eV is assigned to the Pd3d_{3/2}, which also gives an increased binding energy by approximate 2 eV. The increase in BE of Pd(0) arises from the electron transformation from palladium to α -Fe₂O₃ due to the strong interaction between Pd

and α -Fe₂O₃. Fig. 3C shows the X-ray photoelectron spectra signals of the Fe 2p regions, in which the binding energy of Fe 2p_{3/2} is approximate 711eV for Fe³⁺ [41]. The weak satellite peak situated at about 719 eV is a characteristic peak of Fe³⁺ in γ -Fe₂O₃, suggesting a partial formation of γ -Fe₂O₃ during the preparation of Fe₂O₃ powders. The XPS spectra of O1s shown in Fig. 3D are wide and asymmetric, indicating that two kinds of oxygen species are present inside the as-prepared catalyst. Namely, the binding energy of the crystal lattice oxygen (O_{Lat}²⁻) and the oxygen-deficient regions (O_{Def}²⁻) were 529.5 and 531.5 eV, respectively. O_{Lat}²⁻ is attributable to the Fe–O bonding, whereas O_{Def}²⁻ is closely related to the catalytic efficiency of Pd/ α -Fe₂O₃ catalyst.

Further, the area-selected SEM-EDS mapping was performed to determine the Pd, Fe, O element distribution inside the Pd/ α -Fe₂O₃ catalyst (Fig. 4). Fig. 4D shows the element mapping of the carbon in carbon conductive adhesive for the sample preparation. Figures 4E and 4F present the element mappings of α -Fe₂O₃ particles. Moreover, the element mapping of Pd in Fig. 4C suggest a uniform distribution and efficient loading of Pd element on the surface of α -Fe₂O₃.

In addition, the AFM section analysis can be utilized to obtain the size of the nanostructures. Fig. 5 shows the AFM height and topographic phase images of the Pd/ α -Fe₂O₃ particles. The phase image in Fig. 5C indicates that those sample phases are almost uniform and dispersed ball-like particles exhibiting diameters which range from 25 nm to 42 nm. As for the HRTEM image (Fig. 2D), the size of each α -Fe₂O₃ crystal was found to be about 10nm×8nm×8nm. Moreover, the SEM images in Fig. 2B reveal that most of Pd(0.5%)/ α -Fe₂O₃ particles possess average sizes ranged from 1.0 to 1.5 μ m. As a consequence, it is reasonable that these ball-like particles shown in the AFM phase image are indeed the aggregates from α -Fe₂O₃ crystals. The distinguishable information on the particle sizes determined by the three characterizations, *i.e.*, HRTEM, SEM and AFM, probably results from the re-aggregation of those dispersed α -Fe₂O₃ crystals during the ultrasonic processing of the original ethanol solution of the Pd(0.5%)/ α -Fe₂O₃ particles.

3.2 Hydrogenation Performance of o-CNB over Pd/ α -Fe₂O₃ Catalyst

3.2.1 Effect of the Pd Loadings on the Hydrogenation of o-CNB

In this work, the effect of the Pd loadings on the reduction of o-CNB under selected operation conditions was evaluated. Fig. 6 shows the variations of the o-CAN selectivity and the conversion of o-CNB upon the loading content of Pd. It was found that the hydrogenation of o-CNB yields a

4.22% conversion of o-CNB and 95.8% o-CAN selectivity in the absence of Pd. Further, the conversion of o-CNB increased with the loading of Pd, obtaining 100% conversion when the Pd loading content is above 0.5%. However, the o-CAN selectivity displayed a decreased trend increasing Pd content accompanying with an increasing selectivity of AN. This fact probably results from the high activity of Pd resulting in the concomitant dechlorination of

o-CNB, which produces more AN^[42]. Hence, the subsequent o-CNB hydrogenation runs were performed with the Pd/ α -Fe₂O₃ catalyst at a 0.5% Pd loading level.

3.2.2 Effect of the Ratios of o-CNB to Pd(0.5%)/ α -Fe₂O₃

As for a catalytic reaction, it is highly desired to obtain good conversion and selectivity with high substrate/catalyst molar ratios. In the two decades, many groups have studied the hydrogenation of o-CNB with various catalysts, showing o-CNB conversion and o-CAN selectivity. However, previous catalytic hydrogenation runs of o-CNB were carried out at low substrate/catalyst ratios^[43, 44]. In our case, the effect of o-CNB/Pd molar ratios (1000 to 10000) was evaluated for obtaining optimal ratio. The as-prepared Pd(0.5%)/ α -Fe₂O₃ has been found to be obviously effective in the o-CNB hydrogenation with high o-CNB/Pd molar ratios (up to 6000), which is comparable to the hydrogenation of o-CNB promoted by other supported catalysts^[42, 45, 46] including commercial Pd/C^[47, 48].

Fig. 7 indicates that in the ratio range of o-CNB/Pd molar ratios (1000 to 6000) the o-CNB hydrogenation achieved 100% conversion and approximate 90% o-CAN selectivity. With the further increase in molar ratio, a type of inhibition effect was observed for higher substrate (o-CNB) concentration. For instant, the o-CNB conversion with the highest o-CNB/Pd molar ratio (10000:1) is only 0.4 time lower than that with another ratio (6000:1). Based on the general catalytic hydrogenation mechanism, we think that one mainly reason probably result in the declining conversion of o-CNB at high ratios of o-CNB to Pd. That is, substrate molecules with a high concentration competitively inhibit the absorption of hydrogen molecules on the surface of catalyst^[49]. This negative behavior weakened the generation of more active H atoms, greatly impeding the hydrogenation reduction of o-CNB. This trend is highly consistent with

those previous works^[50, 51]. Moreover, the o-CAN selectivity kept a higher value ranging from 89 to 95%, following by a decreased trend of o-CAN selectivity when more than about an o-CNB/Pd molar ratios of 6000. This result is provided an evidence from the dechlorination of o-CNB,

producing more anilines as the main by-product^[39].

3.2.3 Effect of Reaction Temperature on the Hydrogenation of *o*-CNB

Reaction temperature is an important factor that influences the hydrogenation reactivity by controlling reaction route and by changing of catalyst microstructure, or providing extra energy for overcoming the energy barrier. In this case, we have investigated the impact of three different temperatures on the hydrogenation of *o*-CNB promoted by Pd(0.5%)/ α -Fe₂O₃ (Fig. 9). The results in Fig. 9 show that the prepared Pd catalyst was active in the hydrogenation of *o*-CNB, exhibiting an increased conversion as a function of temperature. Nevertheless, no significant differences in *o*-CAN selectivity were observed in the given temperature range. As follows from the data in Fig. 9, it was found that the hydrodehalogenation of *o*-CNB and *o*-CAN was not efficiently inhibited in the *o*-CNB hydrogenation over the as-prepared Pd(0.5%)/ α -Fe₂O₃. This experimental fact probably results from the intrinsic activity of the Pd-base catalyst and the temperature-dependent hydrodehalogenation of *o*-CNB.

Conditions: P_(H₂)=1MPa, t=1h, n_{*o*-CNB}/n_{Pd}=7000:1, V_{ethanol} =5ml.

3.2.4 Dependence of the *o*-CNB Hydrogenation upon Reaction Time

Table 1 presents the variations of *o*-CNB hydrogenation with different reaction times. Under the selected conditions, the conversion of *o*-CNB gradually increased with the increasing reaction time covering a range of 0.5 to 2.0 hours. Based on the hydrogenation pathway, the substrate conversion and product selectivity are correlated to the efficient adsorption on the active catalytic sites^[52]. Prolonging reaction time generally facilitates the interactions between reactants and catalyst. Hence, the present work suggests an increasing tendency of *o*-CNB conversion. Nevertheless, lengthening time brought about a slight lowering of the *o*-CAN selectivity. The main cause probably originates from the further accumulation of more by-products (mainly AN) and intermediates from some side reactions along with the increase of the reaction time. In addition, no other by-product except AN appeared at shorter reaction time (0.5 to 1.5 hrs), suggesting to some extent the Pd-based catalyst used here inhibits the formation of other by-products even if it does not absolutely inhibit the hydrodehalogenation of *o*-CAN. By the way, it is difficult to achieve a high chemoselectivity in ethanol as the solvent in which significant accumulation of intermediates or dechlorination takes place.

3.2.5 Dependence of Hydrogen Pressure on the Reaction Rates

As for the liquid phase hydrogenation reaction, hydrogen content in catalytic system is a vital

factor for the efficient hydrogenation of various compounds [53]. The observations in the present work (Fig. 10) reveal that the conversion of *o*-CNB increased with the increasing hydrogen pressure. The soluble hydrogen in solvent benefits the increase of absorbed hydrogen on the surface of catalyst, improving the interaction with substrate molecules absorbed on the catalyst surface. Therefore, the conversion of *o*-CNB gradually increases (up to 96.3% at 2.0MPa hydrogen pressure) along with increasing hydrogen pressure. Meanwhile, the hydrogenation of *o*-CNB kept relatively stable *o*-CAN selectivity with a region of 81~86 percent. In addition, it is possible to observe that that one side reaction concerning the formation of aniline was reduced as the hydrogen pressure increases. The main reason for this fact consists in the dominate hydrogenation of nitro group over the reductive dechlorination [54] during the hydrogenation of *o*-CNB over α -Fe₂O₃-supported Pd catalyst at high hydrogen pressure.

3.2.6 Recycling Tests

In this work, the stability and recyclability of Pd/ α -Fe₂O₃ for the *o*-CNB hydrogenation was investigated with successive runs under the selected conditions (50⁰C, 1h, $n_{o\text{-CNB}}/n_{\text{Pd}}=1000:1$, $V_{\text{ethanol}}=5\text{ml}$). The solid catalyst was obtained from the reaction mixture by centrifugal separation after each run. The left solid was thoroughly washed with ethanol, and dried in vacuum following by its application in next hydrogenation run. The recycling test was conducted for four times in the present work, totally.

As shown in Fig.11A, the catalyst is relatively stable and no obvious deactivation towards the hydrogenation of *o*-CNB as the Pd-base catalyst was reused three times. Namely, the *o*-CNB hydrogenation is maintained at a higher *o*-CNB conversion (96.34%) and *o*-CAN selectivity (94.44%). Further, the reactivity of the Pd/ α -Fe₂O₃ catalyst sharply decreases at the fourth run revealing approximately one sixth of the initial catalytic activity of the prepared Pd catalyst though 100% selectivity of *o*-CAN was obtained. This observation is probably ascribed to the Pd leaching and the aggregation of Pd/ α -Fe₂O₃ particles. The ICP determination demonstrates Pd leaching with about 0.2% Pd residue, and distinguishable TEM images of original and reused Pd catalysts (Figs. 11B and 11C) indicates the observable aggregation of the Pd-based catalyst during the recycling tests. In addition to above-mentioned factors, the accumulated products (such as AN) of side reactions can bind permanently to a sufficient number of active sites to reduce catalytic efficiency over time, poisoning the Pd/ α -Fe₂O₃ catalyst. In spite of the achieved higher conversion and selectivity for the *o*-CNB hydrogenation after the third test, however, to some extent the UV-light-induced reduced Pd-base catalyst possesses its intrinsic drawback mainly concerning its

slightly fewer reusability. Thus, our next work will focus on the improvement of the reusability of Pd/ α -Fe₂O₃ catalyst.

4. Conclusions

In summary, in the present work the hydrogenation of o-chloronitrobenzene (o-CNB) was investigated over a UV-light reduced Pd-based catalyst loaded on α -Fe₂O₃. The experimental results demonstrate that the light-induced reduction successfully achieved the preparation of α -Fe₂O₃-supported Pd-based catalyst. Furthermore, the as-prepared Pd catalyst exhibited good performance for the hydrogenation of o-CNB, including higher activity and o-CAN reactivity. Under optimum conditions (50°C, 2hrs, P(H₂)=1MPa, n_{o-CNB}/n_{pd}=6000:1, V_{ethanol}=5ml), the conversion of o-CNB and the selectivity of o-CAN reach values respectively up to 100% and 91.4%. Here, the UV-light induced reduction as one convenient method is anticipated to facilitate the preparation of the supported catalysts towards the hydrogenation reactions. Additionally, the further improvement of the stability and activity of supported catalysts based on the UV-light-induced reduction methodology shall be our next project.

Acknowledgement

We gratefully thank financial supports from Key Subject of China Zigong Science & Technology Bureau (No. 2013H07), Key Project of Key Laboratory of Green Catalysis of Sichuan Institutes of High Education (No. LYJ1404). Especially, we highly appreciate Mr. Jinlong Fan as an employee of the Analysis and Testing Center (Sichuan University of Science & Engineering) for his supports in those characterizations, *i.e.*, SEM, AFM and EDS element mapping.

References

1. H.-U. Blaser, H. Steiner, M. Studer. *ChemCatChem*, 2009, 1(2)210-221.
2. B. Nair. *Int. J. Toxicol.*, 2001, 20(Suppl. 3)23-50.
3. A. Stanislaus, B. H. Cooper. *Catal. Rev.*, 1994, 36(1)75-123.
4. P. Serna, A. Corma. *ACS Catal.*, 2015, 5 (12)7114-7121.
5. Y. Y. Chen, C. Wang, H. Y. Liu, J. H. Qiu, X. H. Bao. *Chem. Commun.*, 2005, 5298-5300.
6. F. Cárdenas-Lizana, S. Gómez-Quero, N. Perret, M. A. Keane. *Gold Bull.*, 2009, 42(2) 124-132.
7. G. Y. Fan, W. J. Huang, C. Y. Wang. *Nanoscale*, 2013, 5, 6819-6825.
8. J. Li, X. Y. Shi, Y. Y. Bi, J. F. Wei, Z. G. Chen. *ACS Catal.*, 2011, 1 (6)657-664.
9. R. V. Jagadeesh, T. Stemmler, A. -E. Surkus, H. Junge, K. Junge, M. Beller. *Nature Protocols*, 2015, 10(4)548-557.
10. M. Pietrowski. *Green Chem.*, 2011, 13(7)1633-1635.
11. X. D. Wang, N. Perret, J. J. Delgado, G. Blanco, X. W. Chen, C. M. Olmos, S. Bernal, M. A. Keane. *J. Phys. Chem. C*, 2013, 117(2)994-1005.
12. Z. Z. Wei, J. Wang, S. J. Mao, D. F. Su, H. Y. Jin, Y. H. Wang, F. Xu, H. R. Li, Y. Wang. *ACS Catal.*, 2015, 5 (8)4783-4789.
13. C. Antonetti, M. Oubenali, A. M. R. Galletti, P. Serp, G. Vannucci. *Appl. Catal. A: Gen.*, 2012, 421-422, 99-107.
14. F. Harraz, S. El-Hout, H. Killa, I. Ibrahim. *J. Catal.*, 2012, 286, 184-192.
15. Y. Y. Fang, H. L. Xiao, N. Sui, M. H. Liu, W. W. Yu. *RSC Adv.*, 2014, 4, 11788-11793.
16. F. Cárdenas-Lizana, Y. F. Hao, M. Crespo-Quesada, I. Yuranov, X. D. Wang, M. A. Keane, L. Kiwi-Minsker. *ACS Catal.*, 2013, 3 (6)1386-1396.
17. G. Vilé, N. Almora-Barrios, N. López, J. Pérez-Ramírez. *ACS Catal.*, 2015, 5 (6)3767-3778.
18. P. Lara, K. Philippot. *Catal. Sci. Technol.*, 2014, 4(8)2445-2465.
19. W. T. Zang, G. Z. Li, L. Wang, X. W. Zhang. *Catal. Sci. Technol.*, 2015, 5(5)2532-2553.
20. S. Furukawa, Y. Yoshida, T. Komatsu. *ACS Catal.*, 2014, 4(5)1441-1450.
21. K. Fulajtárova, T. Soták, M. Hronec, I. Vávra, E. Dobročka, M. Omastová. *Appl. Catal. A: Gen.*, 2015, 502, 78-85.
22. J. A. Johnson, J. J. Makis, K. A. Marvin, S. E. Rodenbusch, K. J. Stevenson. *J. Phys. Chem. C*, 2013, 117(44)22644-22651.
23. A. M. R. Galletti, C. Antonetti, A. M. Venezia, G. Giambastiani. *Appl. Catal. A: Gen.*, 2010, 386, 124-131.
24. A. M. R. Galletti, L. Toniolo, C. Antonetti, C. Evangelisti, C. Forte. *Appl. Catal. A: Gen.*, 2012,

- 447-448, 49-59.
25. A. M. R. Galletti, C. Antonetti, M. Bertoldo, F. Piccinelli. *Appl. Catal. A: Gen.*, 2013, 468, 95-101.
 26. C. Antonetti, L. Toniolo, G. Cavinato, C. Forte, C. Ghignoli, R. Ishak, F. Cavani, A. M. R. Galletti. *Appl. Catal. A: Gen.*, 2015, 496, 40-50.
 27. P. Zhang, C. Yu, X. M. Fan, X. N. Wang, Z. Ling, Z. H. Wang, J. S. Qiu. *Phys. Chem. Chem. Phys.*, 2015, 17, 145-150.
 28. W. C. Du, S. X. Xia, R. F. Nie, Z. Y. Hou. *Ind. Eng. Chem. Res.*, 2014, 53(12)4589-4594.
 29. H. M. Liu, H. B. Yu, C. R. Xiong, S. H. Zhou. *RSC Adv.*, 2015, 5, 20238-20247.
 30. U. Jung, A. Elsen, Y. Y. Li, J. G. Smith, M. W. Small, E. A. Stach, A. I. Frenkel, R. G. Nuzzo. *ACS Catal.*, 2015, 5(3)1539-1551.
 31. S. Bhattacharjee, M. L. Bruening. *Langmuir*, 2008, 24(6)2916-2920.
 32. F. A. Harraz, S. E. El-Hout, H. M. Killa, I. A. Ibrahim. *J. Catal.*, 2012, 286, 184-192.
 33. H. Göksu, S. F. Ho, Ö. Metin, K. Korkmaz, A. M. Garcia, M. S. Gültekin, S. H. Sun. *ACS Catal.*, 2014, 4(6)1777-1782.
 34. S. Y. Jung, S. J. Bae, W. J. Lee. *Environ. Sci. Technol.*, 2014, 48(16)9651-9658.
 35. A. M. Alshaibani, Z. Yaakob, A. M. Alsobaai, M. Sahri. *Brazil. J. Chem. Eng.*, 2014, 31(1)69-78.
 36. S. X. Xia, L. P. Zheng, R. F. Nie, P. Chen, H. Lou, Z. Y. Hou. *Chin. J. Catal.*, 2013, 34(5)986-992.
 37. E. Borgarello, N. Serpone, G. Emo, R. Harris, E. Pelizzetti, C. Minero. *Inorg. Chem.*, 1986, 25(25)4499-4503.
 38. S. H. Park, S. H. Kim, S. Y. Park, W. I. Lee, C. M. Lee. *Sensors*, 2014, 14(9) 15849-15860.
 39. K. V. S. Ranganath, J. Kloesges, A. H. Schäfer, F. Glorius. *Angew. Chem. Int. Ed.*, 2010, 49(42)7786-7789.
 40. M. Brun, A. Berthet, J. C. Bertolini. *J. Electron. Spectrosc.*, 1999, 104(1-3)55-60.
 41. P. Li, E. Y. Jiang, H. L. Bai. *J. Phys. D: Appl. Phys.*, 2011, 44(7)075003.
 42. W. W. Lin, J. Zhao, H. Y. Cheng, X. R. Li, X. N. Li, F. Y. Zhao. *J. Colloid Interf. Sci.*, 2014, 432, 200-206.
 43. H. K. Kadam, S. G. Tilve. *RSC Adv.*, 2015, 5, 83391-83407.
 44. Q. Bai, D. Li, L. He, H. L. Xiao, N. Sui, M. H. Liu. *Prog. Nat. Sci. –Mater.*, 2015, 25(3)179-184.
 45. D. Dutta, D. K. Dutta. *Appl. Catal. A: Gen.*, 2014, 487, 158-164.

46. X. D. Wang, F. Cárdenas-Lizana, M. A. Keane. *ACS Sustain. Chem. Eng.*, 2014, 2(12)2781-2789.
47. X. S. Xu, X. Q. Li, H. Z. Gu, Z. B. Huang, X. H. Yan. *Appl. Catal. A: Gen.*, 2012, 429-430, 17-23.
48. Y. L. Xie, N. Xiao, C. Yu, J. S. Qiu. *Catal. Commun.*, 2012, 28, 69-72.
49. U. K. Singh, M. A. Vannice. *Appl. Catal. Part A: Gen.*, 2001, 213(1)1-24.
50. S. Hu, Y. Chen. *Ind. Eng. Chem. Res.*, 1997, 36(12)5153-5159.
51. U. K. Singh, M. A. Vannice. *J. Mol. Catal. Part A: Chem.*, 2000, 163(1-2)233-250.
52. F. Devred, P. Dulgheru, N. Kruse. *Elementary Steps in Heterogeneous Catalysis. Reference Module in Chemistry, Molecular Sciences and Chemical Engineering, from Comprehensive Inorganic Chemistry II (2 Ed.)*, 2013, 7, 7-38.
53. L. Guzzi, Á. Molnár, D. Teschner. *Hydrogenation Reactions: Concepts and Practice. Reference Module in Chemistry, Molecular Sciences and Chemical Engineering, from Comprehensive Inorganic Chemistry II (2 Ed.)*, 2013, 7, 421-457.
54. M. Pietrowski. *Curr. Org. Synth.*, 2012, 9(4)470-487.

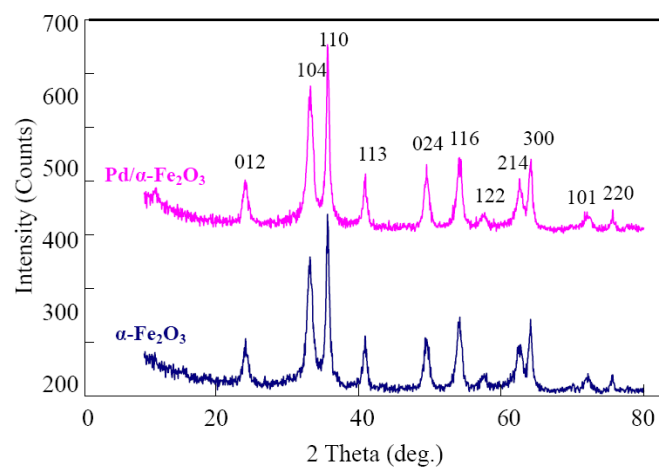


Fig. 1. The XRD patterns of the α -Fe₂O₃ (A) and Pd/ α -Fe₂O₃ catalyst (B).

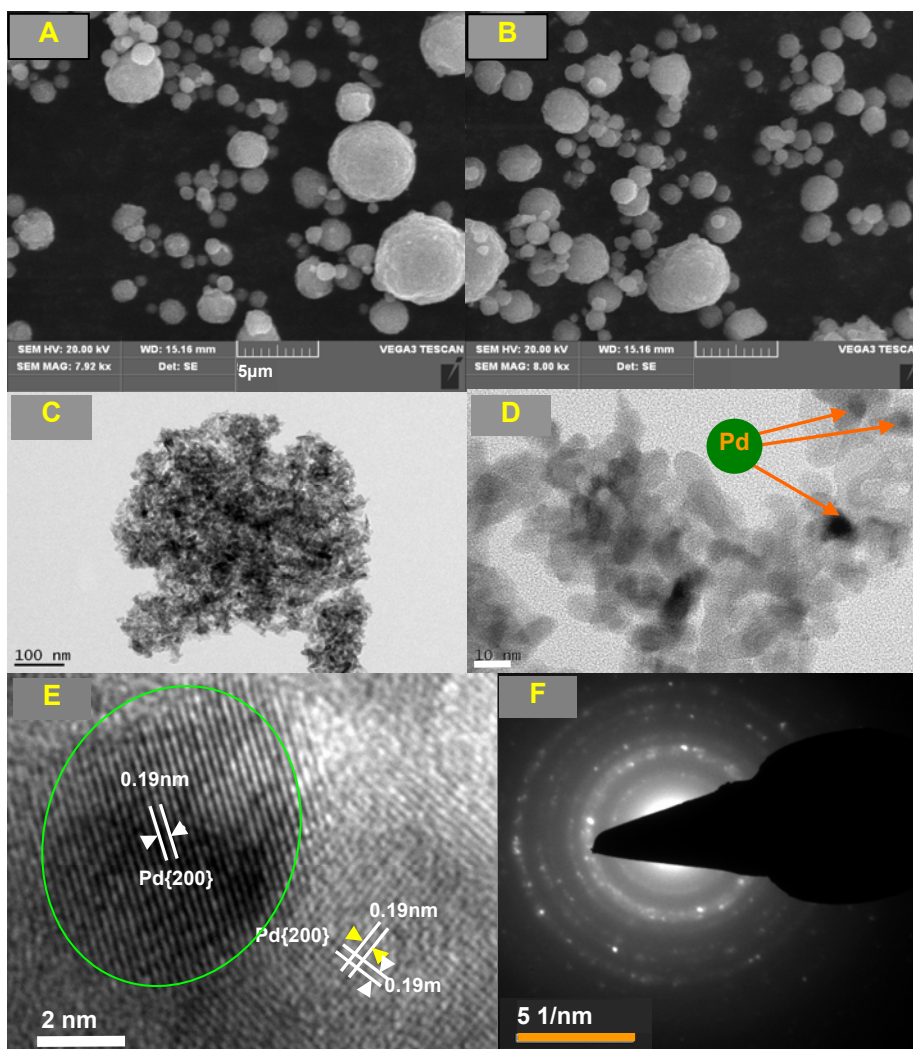


Fig. 2. SEM images of α -Fe₂O₃ (A) and Pd/ α -Fe₂O₃ catalyst with 0.5% Pd theoretical loading (B). Patterns C and D display the TEM patterns of the Pd(0.5%)/ α -Fe₂O₃ catalyst at different scales (100 nm and 10 nm), respectively. Images E and F respectively show the high-resolution TEM and corresponding SAED pattern of Pd(0.5%)/ α -Fe₂O₃ catalyst.

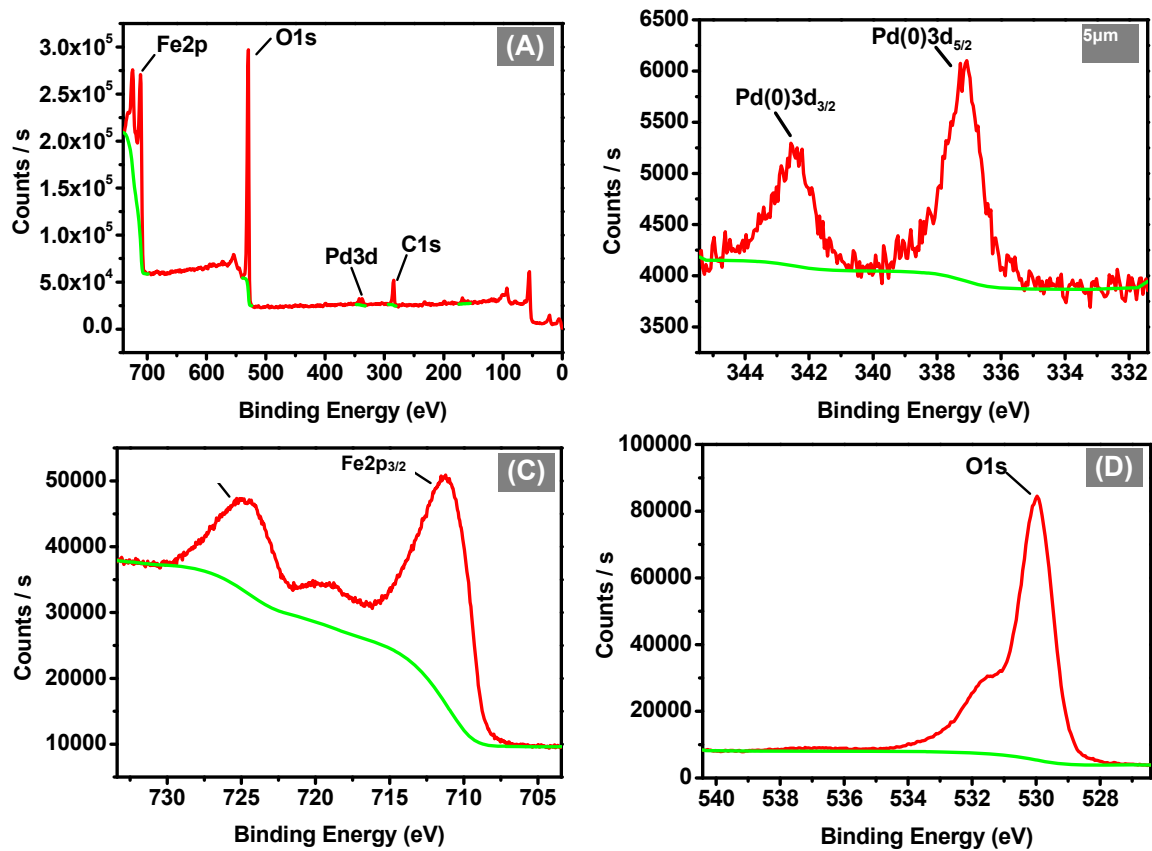


Fig. 3. X-ray photoelectron spectra of the Pd/ α -Fe₂O₃ as catalyst for the hydrogenation of *o*-CNB.

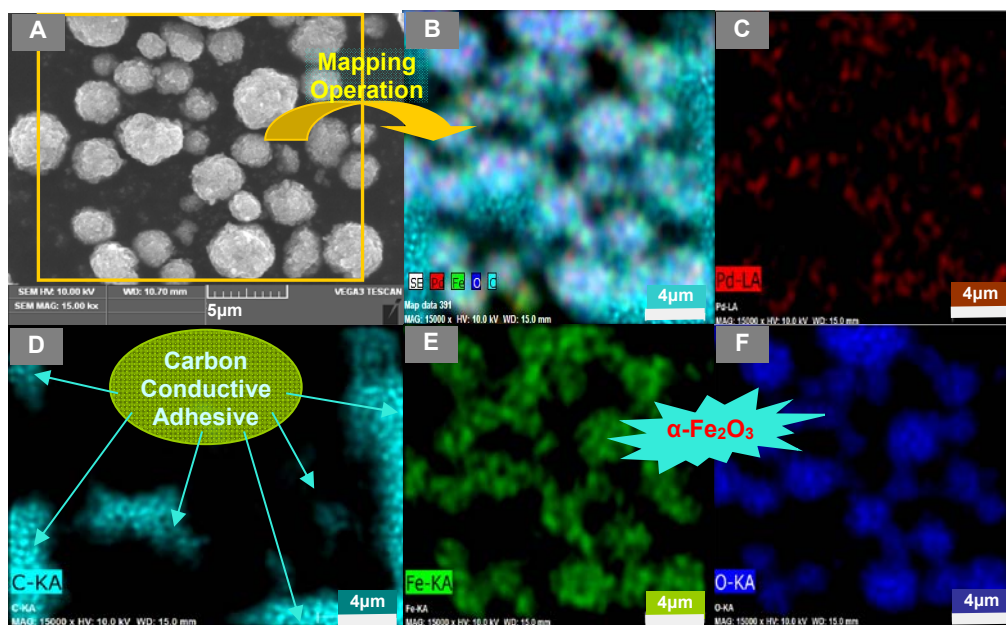


Fig. 4. Scanning electronic micrograph image (A) and corresponding EDS elemental mappings (B-F) of Pd(0.5%)/ α -Fe₂O₃ catalyst in elements of (B) full mapping image, (C) Pd, (D) C (carbon conductive adhesive), (E) Fe, (F) O, respectively.

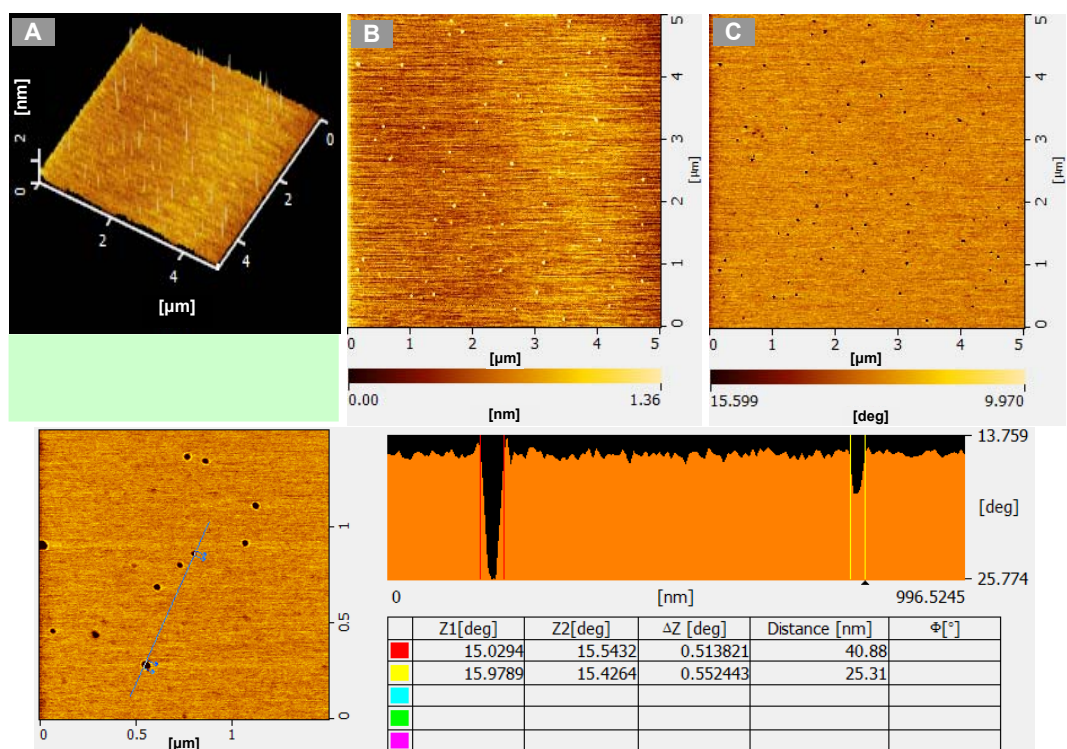


Fig. 5. The AFM 3D view (A), 2D height (B) and topographic phase (C) images of Pd(0.5%)/ α -Fe₂O₃ particles at 5 μm \times 5 μm scale. The lower one shows a phase image of a selected area at a smaller scale level (1.5 μm \times 1.5 μm) compared to the upper one.

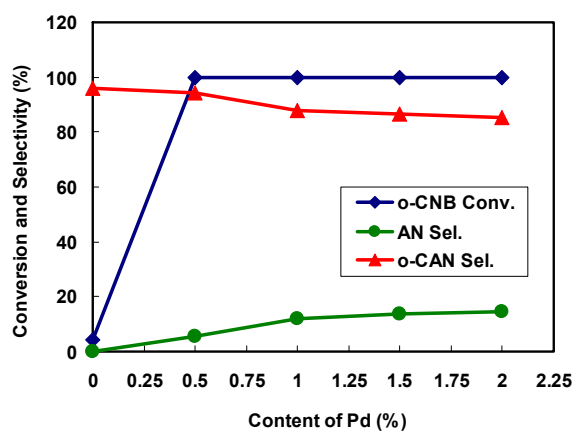


Fig. 6 Variety of the o-CNB hydrogenation as a function of the Pd loadings. Conditions: $T=50^{\circ}\text{C}$, $t=1\text{h}$, $P(\text{H}_2)=1\text{MPa}$, $n_{\text{o-CNB}}/n_{\text{Pd}}=1000:1$, $V_{\text{ethanol}}=5\text{ml}$.

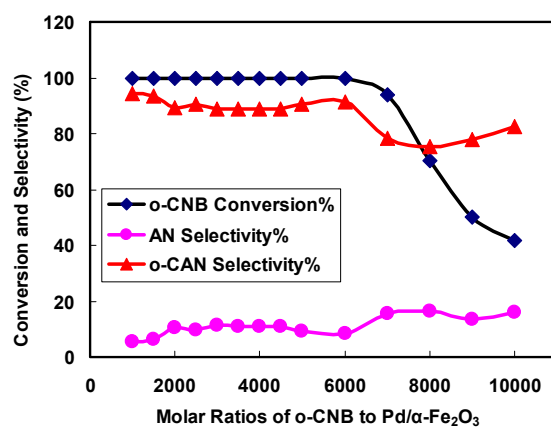


Fig. 7 Dependence of the hydrogenation reduction of o-CNB upon the molar ratios of o-CNB to Pd(0.5%)/α-Fe₂O₃. Conditions: T=50⁰C, t=2h, P(H₂)=1MPa, V_{ethanol}=5ml.

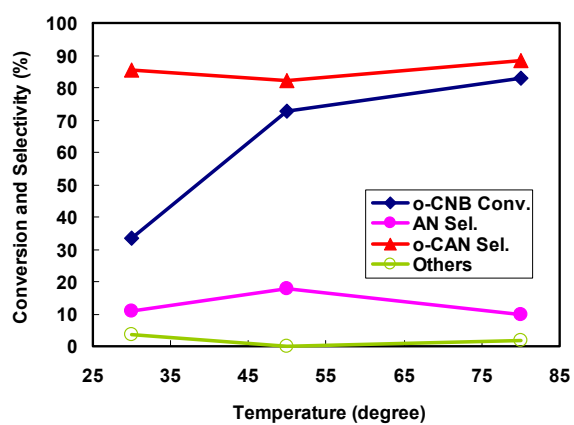


Fig. 9. Effect of temperature on the hydrogenation of o-CNB.

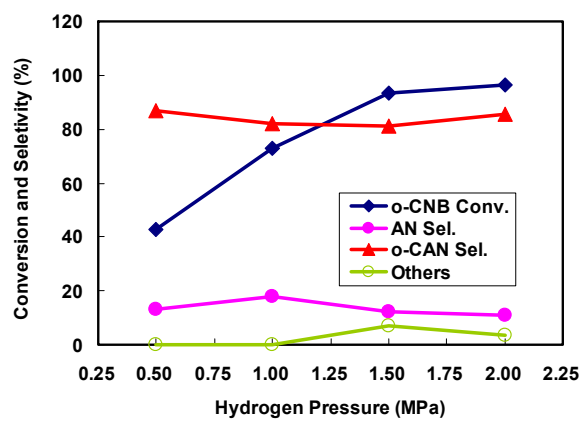


Fig. 10. Dependence of the o-CNB hydrogenation upon the hydrogen pressure. Conditions: $T=50^{\circ}\text{C}$, $t=1\text{h}$, $n_{\text{o-CNB}}/n_{\text{Pd}}=7000:1$, $V_{\text{ethanol}}=5\text{ml}$.

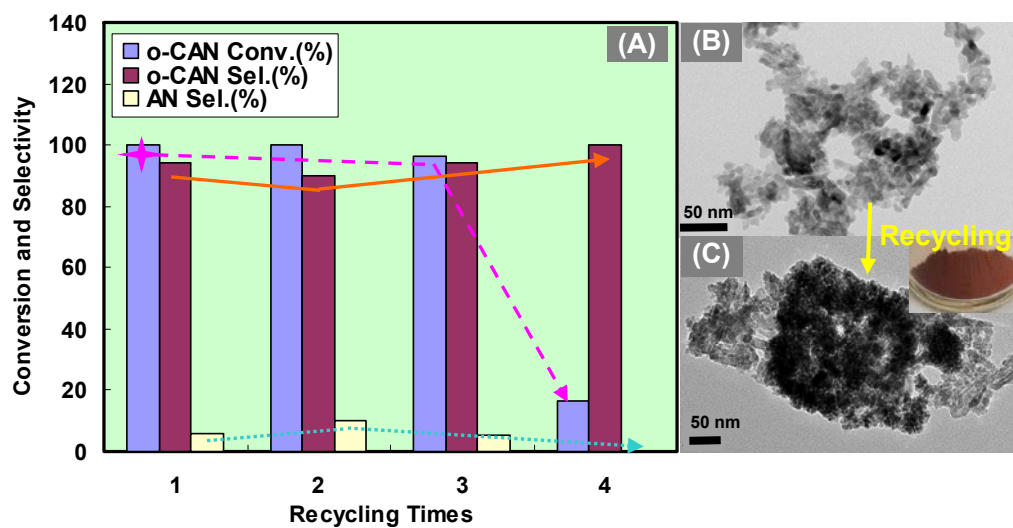
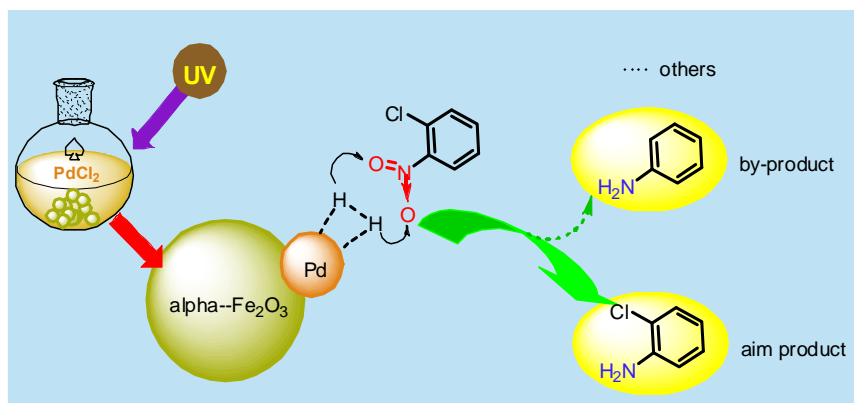


Fig. 11. Recyclability survey (A) of the Pd/ α -Fe₂O₃ catalyst for the hydrogenation of o-CNB. Images B and C shows the TEM images of the initial and reused Pd catalyst, respectively. The insert of Fig. 11C is the reused Pd-based catalyst sample after three runs. Conditions: T=50°C, t=1h, n_{o-CNB}/n_{Pd}=1000:1, V_{ethanol} =5ml.

Scheme



Scheme 1. Representation of the o-CNB hydrogenation by Pd/ $\alpha\text{-Fe}_2\text{O}_3$ catalyst prepared by UV light-induced route.

Table 1 Effect of reaction time on the catalytic hydrogenation of o-CNB

Entry	Reaction time (h)	Conversion (%)	Selectivity (%)		
			o-CAN	AN	Others
1	0.5	41.0	84.7	15.3	-
2	1.0	72.8	82.2	17.8	-
3	1.5	84.7	80.5	16.5	3.0
4	2.0	93.9	78.5	15.4	6.1

Conditions: T=50⁰C, P_(H₂)=1MPa, n_{o-CNB}/n_{Pd}=7000:1, V_{ethanol}=5ml